Stability Constrained Voltage Control in Distribution Grids with Arbitrary Communication Infrastructure

Zhenyi Yuan, *Graduate Student Member, IEEE*, Jie Feng, *Graduate Student Member, IEEE*, Yuanyuan Shi, *Member, IEEE*, and Jorge Cortés, *Fellow, IEEE*

***Abstract*—We consider the problem of designing learning-based reactive power controllers that perform voltage regulation in distribution grids while ensuring closed-loop system stability. In contrast to existing methods, where the provably stable controllers are restricted to be decentralized, we propose a unified design framework that enables the controllers to take advantage of an *arbitrary* communication infrastructure on top of the physical power network. This allows the controllers to incorporate information beyond their local bus, covering existing methods as a special case and leading to less conservative constraints on the controller design. We then provide a design procedure to construct input convex neural network (ICNN) based controllers that satisfy the identified stability constraints by design under arbitrary communication scenarios, and train these controllers using supervised learning. Simulation results on the the University of California, San Diego (UCSD) microgrid testbed illustrate the effectiveness of the framework and highlight the role of communication in improving control performance.**

***Index Terms*—Voltage control, distributed energy resources, closed-loop stability, machine learning.**

I. Introduction

The increasing penetration of distributed energy resources (DERs) poses great challenges to system operations and stability of distribution grids (DGs). For instance, the intermittence of renewable energy sources can lead to rapid and unpredictable fluctuations in the load and generation profiles, causing large voltage variations. This has motivated the study of Volt/Var control strategies which aim to regulate voltages within acceptable preassigned limits by commanding DERs' reactive power injections [1]. However, without appropriate design, the Volt/Var controllers may render the closed-loop system unstable, resulting in voltage oscillations. In this paper, we propose a unified framework to design Volt/Var control strategies that are amenable to DGs with various communication topologies and rigorously guarantee the stability of the closed-loop system.

Literature Review: Initial attempts to ensure closed-loop stability with Volt/Var controllers start from decentralized designs [2]–[5], where the monotonicity of the decentralized controllers is identified as the key property to ensure the asymptotic stability. However, the controller form in these works is constrained to be piece-wise linear, as advocated by the IEEE 1547 Standard [6]. Under these designs, a certain level of steady-state optimality can be achieved only for specific cost function forms. Moreover, the piece-wise linear form of the controllers further prohibits the improvement of performance, and does not take advantage of the fact that inverter-based DERs can implement almost arbitrary control laws thanks to the flexibility in power electronic interfaces.

Motivated by the above factors, recent works [7]–[14] generalize the decentralized Volt/Var controller form to be arbitrary nonlinear, which is more flexible, and still ensure asymptotic stability as long as it satisfies the same monotonicity property. Particularly, machine learning techniques, e.g., reinforcement learning [7]–[10], supervised learning [11]–[13], and unsupervised learning [14], paired with neural network parameterized controllers, are employed to enhance the optimality of controllers. We remark that [7]–[10] focus more on transient performance optimization, while [11]–[14] focus more on steady-state performance.

Beyond decentralized designs, DGs are often equipped with a communication infrastructure on top of the physical network, which allows some buses to exchange information with their neighbors. Motivated by the fact that the optimal power flow (OPF) problem can be solved in a *distributed* fashion under appropriate connectivity conditions on the communication infrastructure, e.g., [15], here we explore distributed designs to enhance the performance of decentralized voltage controllers. Relevant results include [4], [16]–[20], where distributed optimization-based feedback controllers are derived to steer the network toward solutions of OPF. Theoretical results validate the asymptotic convergence of these distributed algorithms, which implies the asymptotic stability of the closed-loop system. However, these algorithms often require that the DGs are endowed with a reliable real-time communication network that is connected and consistent with the physical network, which is rarely satisfied in practice for DGs. While decentralized designs may incorporate optimality considerations, there is significant potential for performance improvement by leveraging available communication infrastructure that may not be consistent with the physical network (or even connected). Hence, instead of asking the controllers to recursively communicate over a restrictive communication network to converge to OPF solutions, here we study the problem of how to take advantage of an arbitrarily existing communication infrastructure to improve performance of the decentralized Volt/Var controllers in DGs by having access to more measurements, so that they behave closer to OPF solutions, and yet ensure closed-loop stability.

Statement of Contributions: We propose a unified framework to design provably stable Volt/Var controllers for DGs with arbitrary communication infrastructures. Specifically, we

This work was supported by NSF Award ECCS-1947050 and ECCS-2200692. The work of J. Feng was supported by the UC-National Laboratory In Residence Graduate Fellowship L24GF7923.

Z. Yuan and J. Cortés are with the Department of Mechanical and Aerospace Engineering, University of California, San Diego, La Jolla, CA 92093, USA, {z7yuan,cortes}@ucsd.edu. J. Feng and Y. Shi are with the Department of Electrical and Computer Engineering, University of California, San Diego, La Jolla, CA 92093, USA, {jif005,yyshi}@ucsd.edu.

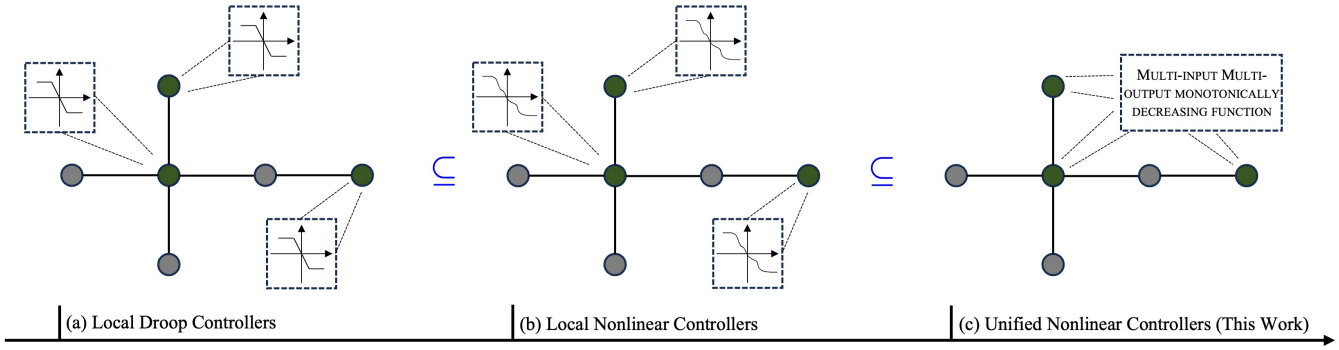

Fig. 1. Road map of Volt/Var control methods with stability guarantees. The green nodes represent the controllable DERs in the DG. The initial attempt on designing provably stable voltage controllers considers the decentralized case, and specifically focuses on piece-wise linear controllers, see panel (a), which include, e.g., earlier works [2]–[5], and is also recently revisited by [21]–[23]. The common requirement for the controller design in these works is the monotonicity constraint. Recent works [7]–[14] then extend the works in panel (a) to the case where these decentralized controllers are not restricted to be piece-wise linear, and instead can be arbitrarily nonlinear. As a consequence, the methods belonging to panel (a) can be viewed as special cases of the methods belonging to panel (b). The proposed framework in this paper improves the methods belonging to panel (b) in the sense that each of the local controllers is not necessarily to be monotonic, instead, it is sufficient to ensure the stability if all the controllers collectively satisfy a network-wise monotonicity constraint. Therefore, the methods belonging to panel (b) can again be viewed as special cases of the methods belonging to panel (c).

obtain an explicit network-wide stability condition on the Volt/Var controllers that ensures the asymptotic stability of the system. This stability condition requires the DERs to collectively satisfy a monotonic constraint, which recovers previous decentralized stability conditions in the literature as special cases, yet is less conservative compared to them. Fig. 1 illustrates the improvement of the proposed framework with respect to existing methods. Moreover, we propose a systematic approach to design local-acting Volt/Var controllers such that they can collectively satisfy this network-wide stability condition. This framework is unified in the sense that each DER only needs to coordinate with its communicating neighbors, regardless of what type of communication infrastructure the DG is endowed with. Finally, we parameterized these controllers as gradient of input convex neural networks (ICNNs) to guarantee monotonicity, and train them via supervised learning. Simulation results on the University of California, San Diego (UCSD) microgrid testbed highlight effectiveness of the proposed framework and the role of communication in improving the performance of voltage controllers.

Notation: Throughout the paper, $\mathbb{R}$ denotes the set of real numbers. Upper and lower case boldface letters denote matrices and column vectors, respectively. Given a matrix $\mathbf{A}$, $\mathbf{A} \succ 0$ denotes that matrix $\mathbf{A}$ is positive definite. We use $\|\cdot\|$ to represent the Euclidean norm, and $|\cdot|$ the cardinality when the argument is a set. We let $\|\mathbf{x}\|_{\mathbf{A}} = \mathbf{x}^\top \mathbf{A}\mathbf{x}$ if $\mathbf{A}$ is square. The symbol $(\cdot)^\top$ stands for transposition, and $\mathbf{1}$ denotes vector of all ones with appropriate dimensions. Operator $\text{Proj}_{\mathcal{X}}(\cdot)$ represents the projection of the argument into the set $\mathcal{X}$.

II. Preliminaries and Problem Formulation

In this section, we introduce the DG model and the communication network, and formulate the problem of interest.

A. Distribution Grid Modeling

A radial single-phase (or a balanced three-phase) DG having $N+1$ buses can be modeled by a tree graph $\mathcal{G} = (\mathcal{N}, \mathcal{E})$ rooted at the substation. The nodes in $\mathcal{N}_0 := \{0, \ldots, N\}$ are associated with grid buses, and the edges in $\mathcal{E}$ with lines. The substation node, labeled as 0, behaves as an ideal voltage source imposing the nominal voltage of 1 p.u. and we let $\mathcal{N} = \mathcal{N}_0 \setminus \{0\}$. We use $\mathbf{M}^0 = [\mathbf{m}_0^\top; \mathbf{M}] \in \mathbb{R}^{(N+1)\times N}$ to denote the incidence matrix of the graph $\mathcal{G}$, where $\mathbf{m}_0^\top$ is the row corresponds to the substation node. The voltage magnitude at bus $n \in \mathcal{N}$ is denoted as $v_n \in \mathbb{R}$, and the active and reactive power injections at bus $n \in \mathcal{N}$ are $p_n, q_n \in \mathbb{R}$, respectively. Powers take positive (negative) values, i.e., $p_n, q_n \geq 0$ ($p_n, q_n \leq 0$), when they are *injected into* (*absorbed from*) the grid. The vectors $\mathbf{v}, \mathbf{p}, \mathbf{q} \in \mathbb{R}^N$ collect the voltage magnitudes, active and reactive power injections for buses $1, 2, \ldots N$. Let (m, n) be an edge in $\mathcal{E}$, let r_{mn} and x_{mn} denote its resistance and reactance, and P_{mn} and Q_{mn} the real and reactive power from bus m to n, respectively. For every line $(m, n) \in \mathcal{E}$, according to the DistFlow equations [24], the power flow model is

$$P_{mn} - \sum_{(n,k)\in\mathcal{E}} P_{nk} = -p_n + r_{mn}\frac{P_{mn}^2 + Q_{mn}^2}{v_m^2}, \tag{1a}$$

$$Q_{mn} - \sum_{(n,k)\in\mathcal{E}} Q_{nk} = -q_n + x_{mn}\frac{P_{mn}^2 + Q_{mn}^2}{v_m^2}, \tag{1b}$$

$$v_m^2 - v_n^2 = 2\left(r_{mn}P_{mn} + x_{mn}Q_{mn}\right) - \left(r_{mn}^2 + x_{mn}^2\right)\frac{P_{mn}^2 + Q_{mn}^2}{v_m^2}. \tag{1c}$$

B. Communication Network

We consider the case where an undirected communication network exists in the DG. We say bus n is a neighbor of bus m if bus m can receive the information broadcasted from bus n. We use $\mathcal{N}_i$ to represent the set of neighbors of bus $i \in \mathcal{N}$. We note that the communication network can be different from the physical network (e.g., buses m and n might be physically connected, but not neighbors of each other in the communication network). In fact, this is a common occurrence due to the fact that DGs are frequently reconfigured [25]. Moreover, we allow the communication

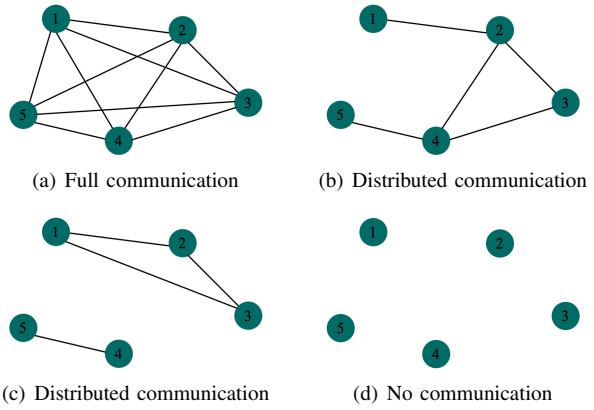

(a) Full communication (b) Distributed communication

(c) Distributed communication (d) No communication

Fig. 2. Examples of different communication infrastructure in DGs, which can be different from the physical power network structure. Note that the difference between (b) and (c) is that the former is connected and the latter is not. Other possible communication situations in DGs can all be viewed as combinations of the above examples, therefore the proposed framework is unified and covers all possible scenarios.

network to be arbitrary and not necessarily connected, i.e., we allow the case that only partial communication is available or even the case that there is no communication at all. Hence, our setting covers all possible communication scenarios in DGs, including, e.g., full communication, distributed communication, and no communication cases, see Fig. 2.

C. Problem Formulation

We are interested in dynamically adjusting the reactive power injections $\{q_i\}_{i\in\mathcal{N}}$ in (1) for the inverter-interfaced DERs to perform voltage regulation in DGs. Specifically, we aim to design, for each $i \in \mathcal{N}$, a function

$$\phi_i : \mathbb{R}^{|\mathcal{N}_i|+1} \to \mathcal{Q}_i,\ \ (v_i, \{v_j\}_{j\in\mathcal{N}_i}) \mapsto \phi_i(v_i, \{v_j\}_{j\in\mathcal{N}_i})$$

that takes accessible voltage magnitude measurements as input and determines its reactive power injection, where $\mathcal{Q}_i := \{q_i \mid q_{i,\min} \le q_i \le q_{i,\max}\}$ defines the reactive power control capability of bus i.

A first consideration for this type of design is how to ensure the stability of the closed-loop dynamics (1) resulting from dynamically adjusting the reactive power injections $\{q_i\}_{i\in\mathcal{N}}$ via the feedback mechanisms $\{\phi_i\}_{i\in\mathcal{N}}$. Related works in the literature, e.g. [7]–[14], consider the case where $\{\phi_i\}_{i\in\mathcal{N}}$ are *decentralized*, i.e., each ϕ_i is a function solely depending on v_i. In general, little is known about how to ensure closed-loop stability for the case when the functions $\{\phi_i\}_{i\in\mathcal{N}}$ are not decentralized and employ other communication infrastructure, cf. Fig. 2. A second consideration is to have the reactive power setpoints determined by $\{\phi_i\}_{i\in\mathcal{N}}$ approximate the OPF solutions for optimality considerations. While solving the OPF problem requires restrictive communication and massive computational resources, it is unrealistic to assign the outputs $\{\phi_i\}_{i\in\mathcal{N}}$ by solving the OPF instances online. Machine learning techniques are often used to find optimal $\{\phi_i\}_{i\in\mathcal{N}}$ offline [7]–[14]. Therefore, it is of interest to figure out how to formulate the learning problem to synthesize desired Volt/Var controllers mimicking the OPF solutions while guaranteeing closed-loop stability. Below we formalize these problems.

Problem II.1. *(Stability constrained voltage control):* Consider the DistFlow model (1) together with $\{\phi_i\}_{i\in\mathcal{N}}$ to determine the reactive power setpoints, our goal is to answer the following two questions:

(Q1) *What conditions on $\{\phi_i\}_{i\in\mathcal{N}}$ are sufficient to guarantee the closed-loop system to be asymptotically stable under arbitrary communication infrastructures?*

(Q2) *How to formulate the learning task to find optimal $\{\phi_i\}_{i\in\mathcal{N}}$ that mimic the OPF solutions while satisfying the stability conditions?*

In the following, we answer (Q1) and (Q2) in Section III and Section IV, respectively.

III. Unified Stability Conditions on Volt/Var Controllers

We consider the following incremental control law for steering the reactive power setpoint to the output of ϕ_i for all $i \in \mathcal{N}$:

$$q_i(t+1) = q_i(t) + \epsilon\Big(\phi_i(v_i(t), \{v_j(t)\}_{j\in\mathcal{N}_i}) - q_i(t)\Big). \quad (2)$$

The parameter $\epsilon \in [0, 1]$ is the stepsize to steer q_i to the output of ϕ_i. Note that this rule is implementable in a distributed fashion over the available communication network. We also remark that given that the output of ϕ_i is constrained to $\mathcal{Q}_i$ for all $i \in \mathcal{N}$, if $q_i(0) \in \mathcal{Q}_i$, then we have $q_i(t) \in \mathcal{Q}_i$ for all $t \ge 0$ as the new reactive power setpoint would be the convex combination of two points belong to $\mathcal{Q}_i$. Throughout the paper, we assume that $q_i(0) \in \mathcal{Q}_i$ for all $i \in \mathcal{N}$.

We consider the linearized version (LinDistFlow) [3] of (1) for ease of theoretical analysis of system stability:

$$P_{mn} - \sum_{(n,k)\in\mathcal{E}} P_{nk} = -p_n, \quad (3a)$$

$$Q_{mn} - \sum_{(n,k)\in\mathcal{E}} Q_{nk} = -q_n, \quad (3b)$$

$$v_m - v_n = r_{mn}P_{mn} + x_{mn}Q_{mn}, \quad (3c)$$

which can be written in the following compact form

$$\mathbf{v} = \mathbf{R}\mathbf{p} + \mathbf{X}\mathbf{q} + \mathbf{1}. \quad (4)$$

Here, $\mathbf{R} = \mathbf{M}^{-\top}\mathbf{D}_r\mathbf{M}^{-1}$ and $\mathbf{X} = \mathbf{M}^{-\top}\mathbf{D}_x\mathbf{M}^{-1}$, where $\mathbf{D}_r, \mathbf{D}_x \in \mathbb{R}^{N\times N}$ are diagonal matrices which respectively collect r_{mn} and x_{mn} for all $(m, n) \in \mathcal{E}$. Particularly, we have that $\mathbf{X}, \mathbf{R} \succ 0$, cf. [3].

Collecting $\{\phi_i\}_{i\in\mathcal{N}}$ into $\boldsymbol{\phi}$, and adopting the linearized power flow equation (4), we obtain the closed-loop system dynamics in the following compact form:

$$\mathbf{q}(t+1) = \mathbf{q}(t) + \epsilon\left(\boldsymbol{\phi}(\mathbf{v}(t)) - \mathbf{q}(t)\right), \quad (5a)$$

$$\mathbf{v}(t+1) = \mathbf{X}\mathbf{q}(t+1) + \hat{\mathbf{v}}, \quad (5b)$$

where it is tacitly assumed that the variability of $\mathbf{p}$ is at a much slower timescale than the above iterates, thus the $\mathbf{p}$ remains a constant term during the convergence of the iterations of (5). leading to a fixed $\hat{\mathbf{v}} = \mathbf{R}\mathbf{p} + \mathbf{1}$ in convergence analysis of (5).

From (5), it is easy to see that an equilibrium point $(\mathbf{v}^\star, \mathbf{q}^\star)$ should satisfy

$$\boldsymbol{\phi}(\mathbf{v}^\star) = \mathbf{q}^\star,\ \ \mathbf{v}^\star = \mathbf{X}\mathbf{q}^\star + \hat{\mathbf{v}}, \quad (6)$$

and thus, consistently with our prior work [11], [12], we refer $\{\phi_i\}_{i\in\mathcal{N}}$ to as *equilibrium functions*.

Remark III.1. *(Local asymptotic stability of the original nonlinear dynamics):* In the closed-loop stability analysis here, we rely on the linearized power flow model (5b), which is common in the existing works on reactive power control, see e.g. [2]–[5]. We emphasize that, although the linearization of the power flow model adds limitations to the theoretical results itself, the global asymptotic stability of the closed-loop system with linearized power flow model (as we will show later) still implies local asymptotic stability of the closed-loop system with original nonlinear power flow model in (1). We leave the characterization of the region of attraction for future work. •

A. Existence and Uniqueness of the Equilibrium

Here, we study the properties of equilibrium points of the closed-loop system (5). The following result identifies a sufficient condition on these equilibrium functions so that there exists a unique equilibrium point.

Proposition III.2. *(Existence and uniqueness of the equilibrium): Consider the closed-loop system (5). If $\boldsymbol{\phi}$ is a monotonically decreasing function w.r.t. $\mathbf{v}$, i.e.,*

$$\left(\boldsymbol{\phi}(\mathbf{v})-\boldsymbol{\phi}(\mathbf{v}')\right)^\top(\mathbf{v}-\mathbf{v}')\le 0, \tag{7}$$

or equivalently,

$$\sum_{i\in\mathcal{N}}\left(\phi_i(v_i,\{v_j\}_{j\in\mathcal{N}_i})-\phi_i(v_i',\{v_j'\}_{j\in\mathcal{N}_i})\right)(v_i-v_i')\le 0 \tag{8}$$

holds $\forall\ \mathbf{v},\mathbf{v}'\in\mathbb{R}^N$, then (5) admits a unique equilibrium.

Proof. We first show the existence of the equilibrium. From (6), the closed-loop system (5) admits an equilibrium if there exists a fixed point to

$$\mathbf{q}=\boldsymbol{\phi}(\mathbf{X}\mathbf{q}+\hat{\mathbf{v}})=\tilde{\boldsymbol{\phi}}(\mathbf{q}).$$

where $\tilde{\boldsymbol{\phi}}:\mathcal{Q}\mapsto\mathcal{Q}$. According to Brouwer's Fixed Point Theorem [26, Corollary 6.6], since $\mathcal{Q}$ is convex and compact, such fixed point must exist.

Now we show the uniqueness of the equilibrium, and we reason by contradiction. Suppose there exist two equilibrium points for (5), namely $(\mathbf{q}^*,\mathbf{v}^*)$ and $(\mathbf{q}^\sharp,\mathbf{v}^\sharp)$, with $\mathbf{v}^*\neq\mathbf{v}^\sharp$. From (6), $\boldsymbol{\phi}(\mathbf{v}^*)=\mathbf{q}^*$ and $\boldsymbol{\phi}(\mathbf{v}^\sharp)=\mathbf{q}^\sharp$ hold. Therefore,

$$\mathbf{q}^*-\mathbf{q}^\sharp=\boldsymbol{\phi}(\mathbf{v}^*)-\boldsymbol{\phi}(\mathbf{v}^\sharp). \tag{9}$$

From this, we deduce that

$$(\mathbf{v}^*-\mathbf{v}^\sharp)^\top(\mathbf{q}^*-\mathbf{q}^\sharp)=(\mathbf{v}^*-\mathbf{v}^\sharp)^\top\left(\boldsymbol{\phi}(\mathbf{v}^*)-\boldsymbol{\phi}(\mathbf{v}^\sharp)\right)\le 0,$$

where we have leveraged the monotonicity property (7). On the other hand, it follows from (6) that $\mathbf{v}^*-\mathbf{v}^\sharp=\mathbf{X}(\mathbf{q}^*-\mathbf{q}^\sharp)$, and thus

$$\mathbf{q}^*-\mathbf{q}^\sharp=\mathbf{X}^{-1}(\mathbf{v}^*-\mathbf{v}^\sharp), \tag{10}$$

which implies that

$$(\mathbf{v}^*-\mathbf{v}^\sharp)^\top(\mathbf{q}^*-\mathbf{q}^\sharp)=(\mathbf{v}^*-\mathbf{v}^\sharp)^\top\mathbf{X}^{-1}(\mathbf{v}^*-\mathbf{v}^\sharp)>0,$$

leading to a contradiction. □

B. Global Asymptotic Stability of the Equilibrium

Given the fact that the closed-loop system (5) admits a unique equilibrium under Proposition III.2, we provide in the next result a sufficient condition on ϵ such that this unique equilibrium point is globally asymptotically stable.

Theorem III.3. *(Global asymptotic stability of the equilibrium): Consider the closed-loop system (5) and let $\boldsymbol{\phi}$ be monotonically decreasing function w.r.t. $\mathbf{v}$, cf. (7). If ϵ satisfies*

$$\epsilon<\min\left\{1,\frac{2}{1+L^2\|\mathbf{X}\|^2}\right\}, \tag{11}$$

where $L=\max\limits_{x,y\in\mathcal{B}}\frac{\|\boldsymbol{\phi}(x)-\boldsymbol{\phi}(y)\|}{\|x-y\|}$, with $\mathcal{B}\in\mathbb{R}^{|\mathcal{N}|}$ an arbitrarily large compact set. Then (5) admits a unique equilibrium which is globally asymptotically stable.

Proof. According to Proposition III.2, there exists a unique equilibrium $(\mathbf{q}^\star,\mathbf{v}^\star)$ for (5). Consider the following discrete-time Lyapunov function

$$D(t)=\|\mathbf{v}(t)-\mathbf{v}^\star\|_{\mathbf{X}^{-1}}, \tag{12}$$

which measures the distance between $\mathbf{v}(t)$ and the equilibrium $\mathbf{v}^\star$. It then follows that

$$\begin{aligned}
&D(t+1)\\
&=\|\mathbf{v}(t+1)-\mathbf{v}^\star\|_{\mathbf{X}^{-1}}\\
&=\|\mathbf{X}\left(\mathbf{q}(t)+\epsilon\left(\boldsymbol{\phi}(\mathbf{v}(t))-\mathbf{q}(t)\right)\right)+\hat{\mathbf{v}}-\mathbf{v}^\star\|_{\mathbf{X}^{-1}}\\
&=\|(1-\epsilon)\mathbf{X}\mathbf{q}(t)+\epsilon\mathbf{X}\boldsymbol{\phi}(\mathbf{v}(t))+\hat{\mathbf{v}}-\mathbf{v}^\star\|_{\mathbf{X}^{-1}}\\
&=\|(1-\epsilon)(\mathbf{v}(t)-\mathbf{v}^\star)+\epsilon(\mathbf{X}\boldsymbol{\phi}(\mathbf{v}(t))+\hat{\mathbf{v}}-\mathbf{v}^\star)\|_{\mathbf{X}^{-1}}\\
&=\|(1-\epsilon)(\mathbf{v}(t)-\mathbf{v}^\star)+\epsilon\mathbf{X}\left(\boldsymbol{\phi}(\mathbf{v}(t))-\boldsymbol{\phi}(\mathbf{v}^\star)\right\|_{\mathbf{X}^{-1}},
\end{aligned}$$

where we use the fact $\mathbf{v}^\star=\mathbf{X}\mathbf{q}^\star+\hat{\mathbf{v}}=\mathbf{X}\boldsymbol{\phi}(\mathbf{v}^\star)+\hat{\mathbf{v}}$ in the last equality. Expanding this expression,

$$\begin{aligned}
D(t+1)=&(1-\epsilon)^2\|\mathbf{v}(t)-\mathbf{v}^\star\|_{\mathbf{X}^{-1}}\\
&+2\epsilon(1-\epsilon)\left(\boldsymbol{\phi}(\mathbf{v}(t))-\boldsymbol{\phi}(\mathbf{v}^\star)\right)^\top(\mathbf{v}(t)-\mathbf{v}^\star)\\
&+\epsilon^2\|\boldsymbol{\phi}(\mathbf{v}(t))-\boldsymbol{\phi}(\mathbf{v}^\star)\|_{\mathbf{X}}.
\end{aligned}$$

Therefore, leveraging the monotonicity property (7), we have

$$\begin{aligned}
&D(t+1)-D(t)\\
&=\epsilon(\epsilon-2)\|\mathbf{v}(t)-\mathbf{v}^\star\|_{\mathbf{X}^{-1}}+\epsilon^2\|\boldsymbol{\phi}(\mathbf{v}(t))-\boldsymbol{\phi}(\mathbf{v}^\star)\|_{\mathbf{X}}\\
&\quad+\underbrace{2\epsilon(1-\epsilon)\left(\boldsymbol{\phi}(\mathbf{v}(t))-\boldsymbol{\phi}(\mathbf{v}^\star)\right)^\top(\mathbf{v}(t)-\mathbf{v}^\star)}_{\le 0}\\
&\le\epsilon(\epsilon-2)\|\mathbf{v}(t)-\mathbf{v}^\star\|_{\mathbf{X}^{-1}}+\epsilon^2\|\boldsymbol{\phi}(\mathbf{v}(t))-\boldsymbol{\phi}(\mathbf{v}^\star)\|_{\mathbf{X}}.
\end{aligned}$$

We show next that $D(t+1)-D(t)<0$ for all $t\ge 0$ whenever $\mathbf{v}(t)\neq\mathbf{v}^\star$, which implies the global asymptotic stability of the equilibrium. It is straightforward to see that, for this inequality to hold, it is sufficient to ask that

$$\epsilon<\min_{t\ge 0}\left\{\frac{2\|\mathbf{v}(t)-\mathbf{v}^\star\|_{\mathbf{X}^{-1}}}{\|\mathbf{v}(t)-\mathbf{v}^\star\|_{\mathbf{X}^{-1}}+\|\boldsymbol{\phi}(\mathbf{v}(t))-\boldsymbol{\phi}(\mathbf{v}^\star)\|_{\mathbf{X}}}\right\}, \tag{13}$$

which is equivalent to

$$\frac{1}{\epsilon}>\max_{t\ge 0}\left\{\frac{\|\mathbf{v}(t)-\mathbf{v}^\star\|_{\mathbf{X}^{-1}}+\|\boldsymbol{\phi}(\mathbf{v}(t))-\boldsymbol{\phi}(\mathbf{v}^\star)\|_{\mathbf{X}}}{2\|\mathbf{v}(t)-\mathbf{v}^\star\|_{\mathbf{X}^{-1}}}\right\}.$$

Note that $\|\boldsymbol{\phi}(\mathbf{v}(t))-\boldsymbol{\phi}(\mathbf{v}^\star)\|_{\mathbf{X}} \le L^2\|\mathbf{X}\|\|\mathbf{v}(t)-\mathbf{v}^\star\|^2$, while $\|\mathbf{v}(t)-\mathbf{v}^\star\|_{\mathbf{X}^{-1}} \ge \|\mathbf{X}\|^{-1}\|\mathbf{v}(t)-\mathbf{v}^\star\|^2$. It follows that

$$\max_{t\ge 0}\left\{\frac{\|\mathbf{v}(t)-\mathbf{v}^\star\|_{\mathbf{X}^{-1}}+\|\left(\boldsymbol{\phi}(\mathbf{v}(t))-\boldsymbol{\phi}(\mathbf{v}^\star)\right\|_{\mathbf{X}}}{2\|\mathbf{v}(t)-\mathbf{v}^\star\|_{\mathbf{X}^{-1}}}\right\} \le \frac{1}{2}+\frac{L^2\|\mathbf{X}\|}{2\|\mathbf{X}\|^{-1}} \le \frac{1+L^2\|\mathbf{X}\|^2}{2}.$$

Therefore, $\epsilon < \frac{2}{1+L^2\|\mathbf{X}\|^2}$ is sufficient to make sure (13) hold. This, together with $\epsilon \in [0,1]$, completes the proof. □

Theorem III.3 indicates that given $\boldsymbol{\phi}$ is a monotonic function w.r.t. $\mathbf{v}$, one can always find a small enough ϵ such that the closed-loop system is globally asymptotically stable under (2). The upper bound of ϵ relies on the network parameter $\|\mathbf{X}\|$ and the Lipschitz constant L for selected $\boldsymbol{\phi}$, which can be easily computed offline before the online implementation of the controllers. Or one can continuously scale down ϵ during the online implementation until the controllers work well.

Remark III.4. *(Less conservative stability conditions compared to prior work and the role of communication in improving performance):* Previous works [9]–[12] have identified properties on decentralized voltage controllers to ensure closed-loop stability. Considering the same incremental update rule as (2), the proof techniques in these works would amount to the following inequality for each bus to ensure closed-loop stability in the context of this work:

$$\left(\phi_i(v_i,\{v_j\}_{j\in\mathcal{N}_i})-\phi_i(v_i',\{v_j'\}_{j\in\mathcal{N}_i})\right)(v_i-v_i') \le 0, \quad (14)$$

for all $i \in \mathcal{N}$ and $\mathbf{v},\mathbf{v}' \in \mathbb{R}^N$, i.e., a monotonicity condition for decentralized controller at each bus $i \in \mathcal{N}$. These conditions imply (7), but not the other way around. Thus, the condition obtained in this paper is more general.

In fact, for our proposed framework, the condition is relaxed such that the controllers are only required to collectively satisfy the monotonicity condition. For instance, condition (7) is satisfied if

$$\left(\phi_i(v_i,\{v_j\}_{j\in\mathcal{N}_i})-\phi_i(v_i',\{v_j'\}_{j\in\mathcal{N}_i})\right)(v_i-v_i') \le b_i, \quad (15a)$$

$$\sum_{i\in\mathcal{N}} b_i = 0. \quad (15b)$$

This allows some buses to violate (14) up to a level that can be compensated by other buses to still make the overall summation (8) non-positive. We can think of $\{b_i\}_{i\in\mathcal{N}}$ as *budgets*, cf. [27], that allow us to make the stability condition less conservative. The condition (14) turns out to be a special case of (15) with $\{b_i\}_{i\in\mathcal{N}}$ all zero.

This comparison also highlights the value of the role of communication: (15b) can be enforced via coordination among buses with non-zero b_i's, providing more flexibility to improve the overall performance. Another important observation is that, unlike most of the existing voltage controller designs, e.g., [3], [6], [28], our framework here allows the controller at each bus $i \in \mathcal{N}$ to not be necessarily monotonic w.r.t. its local voltage magnitude, while still guaranteeing closed-loop stability. We envision this is particularly meaningful in the design of provably stable voltage controllers for DGs with relatively small capable DERs, and in scenarios where the system operator aims on minimizing power losses instead of voltage deviations, as in such cases the monotonicity requirement on every bus might be the main source of conservativeness [13]. •

C. The Case When Only a Subset of Buses Are Controllable

The framework we introduce above assumes that all the buses are equipped with DERs that are able to perform reactive power control. However, in some scenarios, there might exist buses which are load buses and have no voltage control capability. We show here how these scenarios can also be covered by our design: as long as the controllable buses satisfy the monotonicity requirement (8), the stability condition (7) holds automatically. To be more specific, let $\mathcal{C} \subseteq \mathcal{N}$ and $\mathcal{U} := \mathcal{N} \setminus \mathcal{C}$ denote the sets of controllable buses and uncontrollable buses, respectively. It is easy to see that the power flow equation (4) can be partitioned as

$$\begin{bmatrix}\mathbf{v}_{\mathcal{U}}\\ \mathbf{v}_{\mathcal{C}}\end{bmatrix} = \begin{bmatrix}\mathbf{R}_{\mathcal{U}\mathcal{U}} & \mathbf{R}_{\mathcal{U}\mathcal{C}}\\ \mathbf{R}_{\mathcal{U}\mathcal{C}}^\top & \mathbf{R}_{\mathcal{C}\mathcal{C}}\end{bmatrix}\begin{bmatrix}\mathbf{p}_{\mathcal{U}}\\ \mathbf{p}_{\mathcal{C}}\end{bmatrix} + \begin{bmatrix}\mathbf{X}_{\mathcal{U}\mathcal{U}} & \mathbf{X}_{\mathcal{U}\mathcal{C}}\\ \mathbf{X}_{\mathcal{U}\mathcal{C}}^\top & \mathbf{X}_{\mathcal{C}\mathcal{C}}\end{bmatrix}\begin{bmatrix}\mathbf{q}_{\mathcal{U}}\\ \mathbf{q}_{\mathcal{C}}\end{bmatrix} + \mathbf{1},$$

where $\mathbf{R}_{\mathcal{U}\mathcal{U}}, \mathbf{R}_{\mathcal{C}\mathcal{C}}, \mathbf{X}_{\mathcal{U}\mathcal{U}}, \mathbf{X}_{\mathcal{C}\mathcal{C}} \succ 0$ [29] and it follows that

$$\mathbf{v}_{\mathcal{C}} = \mathbf{X}_{\mathcal{C}\mathcal{C}}\mathbf{q}_{\mathcal{C}} + \tilde{\mathbf{v}}, \quad (16)$$

in which $\tilde{\mathbf{v}} = \mathbf{R}_{\mathcal{U}\mathcal{C}}^\top\mathbf{p}_{\mathcal{U}} + \mathbf{R}_{\mathcal{C}\mathcal{C}}\mathbf{p}_{\mathcal{C}} + \mathbf{X}_{\mathcal{U}\mathcal{C}}^\top\mathbf{q}_{\mathcal{U}} + \mathbf{1}$. Therefore, one can derive the closed-loop system dynamics in the same form as (5), and thus our theoretical results keep valid.

IV. Learning Stable Voltage Controllers under Arbitrary Communication Infrastructures

Given the identified constraints on $\{\phi_i\}_{i\in\mathcal{N}}$ to ensure the closed-loop system stability, here we are interested in developing a data-driven framework for synthesizing optimal $\{\phi_i\}_{i\in\mathcal{N}}$ which satisfy the stability constraints by design given an arbitrary communication infrastructure. This gives rise to the following optimization problem:

$$\min_{\{\phi_i\}_{i\in\mathcal{N}}} \sum_{k=1}^{K}\sum_{t=0}^{T-1} f(\mathbf{p}^k,\mathbf{q}(t)) \quad (17a)$$

$$\text{s.t. Power Flow Model (1)} \quad (17b)$$

$$\mathbf{q}(t+1) = \mathbf{q}(t) + \epsilon\left(\boldsymbol{\phi}(\mathbf{v}(t)) - \mathbf{q}(t)\right) \quad (17c)$$

$$\boldsymbol{\phi} \text{ is monotone w.r.t. } \mathbf{v} \quad (17d)$$

$$\boldsymbol{\phi} \in \mathcal{Q} := \times_{i\in\mathcal{N}}\mathcal{Q}_i \quad (17e)$$

where we aim to optimize the cost function of interest $f : \mathbb{R}^{2N} \mapsto \mathbb{R}$ in (17a) for a total of K load-generation scenarios, with T the transient time horizon for each scenario. A common choice of the cost function f is the penalization on the voltage deviation from desired limits, i.e., $\|\mathbf{v}(\mathbf{p}^k,\mathbf{q}(t)) - \mathbf{1}\|$. Other formulations may consider electric losses in the network or the deviation from a pre-determined substation power trajectory. The constraint (17e) defines the capability of reactive power compensation, while the constraints in (17d) ensure that the designed controllers render the closed-loop system globally asymptotically stable to a unique equilibrium, cf. Theorem III.3. The optimization problem (17) is not amenable to relevant learning algorithms because of the constraint (17d), which restricts the behavior of the control policy to be learned.

Similar to our prior works [9], [12], the idea to solve (17) is to construct structured neural networks for parameterizing $\{\phi_i\}_{i\in\mathcal{N}}$ such that (17d) is satisfied by design. Unlike

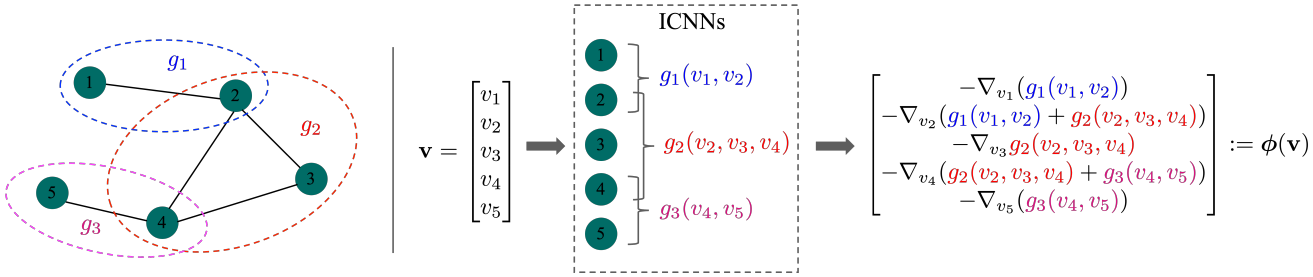

Fig. 3. Illustration of the proposed design procedure to compute equilibrium functions under the distributed communication infrastructure example in Fig. 2(b).

the decentralized case in [9], [12], where each $\{\phi_i\}_{i\in\mathcal{N}}$ is simply paramterized by a single-input single-output monotone Rectified Linear Unit (ReLU) neural network, here we focus on the case that there is a communication infrastructure that allows $\{\phi_i\}_{i\in\mathcal{N}}$ to coordinate with each other to satisfy the less-conservative *collective monotone* requirement (7). In the next, we draw inspirations from [30] and propose the following unified design procedure to achieve this under arbitrary communication infrastructure leveraging Input convex neural network (ICNN) [31], which involves the following steps.

Step 1: Communication network partition: Partition the communication graph into subgraphs such that the buses in each subgraph are all-to-all connected. Note that one bus may appear in multiple subgraphs.

Step 2: ICNN for each subgraph: Suppose there are in total S subgraphs indexed by $\mathcal{S} \triangleq \{1, ..., S\}$ and the ℓ-th subgraph contains buses $\mathcal{M}_\ell \subseteq \mathcal{N}$. Design ICNNs $g_\ell : \mathbb{R}^{|\mathcal{M}_\ell|} \to \mathbb{R}$ for all $\ell \in \mathcal{S}$, where the inputs are voltage magnitude measurements from the buses in the ℓ-th subgraph.

Step 3: Derivation of $\{\phi_i\}_{i\in\mathcal{N}}$ through computing gradients of ICNNs: For each $i \in \mathcal{N}$, let $\boldsymbol{\phi}(\mathbf{v}) := -\sum_{\ell\in\mathcal{S}} \nabla_{\mathbf{v}} g_\ell(\mathbf{v})$.

We emphasize that this procedure is naturally suitable for different communication scenarios, as every bus only uses the information available from itself as well as its communicating neighbors to determine its equilibrium function. To be more illustrative, we show in Fig. 3 how this procedure works for the distributed communication infrastructure displayed in Fig. 2(b). We note that the design procedure works similarly for other arbitrary communication infrastructures. In the next result, we provide a formal result that verifies this design procedure yields equilibrium functions that satisfy (7).

Proposition IV.1. *(Unified equilibrium function design procedure): Given that all the functions $\{g_\ell\}_{\ell\in\mathcal{S}}$ are convex, the obtained equilibrium functions $\{\phi_i\}_{i\in\mathcal{N}}$ are guaranteed to satisfy (7) under arbitrary communication infrastructure.*

Proof. It follows that

$$\begin{aligned}
&\left(\boldsymbol{\phi}(\mathbf{v}) - \boldsymbol{\phi}(\mathbf{v}')\right)^\top (\mathbf{v} - \mathbf{v}') \\
&= -\Big(\sum_{\ell\in\mathcal{S}} \nabla_{\mathbf{v}} g_\ell(\mathbf{v}) - \sum_{\ell\in\mathcal{S}} \nabla_{\mathbf{v}} g_\ell(\mathbf{v}')\Big)(\mathbf{v} - \mathbf{v}') \\
&= -\sum_{\ell\in\mathcal{S}} \left(\nabla_{\mathbf{v}} g_\ell(\mathbf{v}) - \nabla_{\mathbf{v}} g_\ell(\mathbf{v}')\right)(\mathbf{v} - \mathbf{v}').
\end{aligned}$$

Since g_ℓ is convex for all $\ell \in \mathcal{S}$, it holds that $-\left(\nabla_{\mathbf{v}} g_\ell(\mathbf{v}) - \nabla_{\mathbf{v}} g_\ell(\mathbf{v}')\right)^\top (\mathbf{v} - \mathbf{v}') \leq 0$, we conclude that (7) is satisfied. □

Given Proposition IV.1, we are now able to rewrite the optimization problem (17) into the following learning-amenable form[1]:

$$\min_{\{\alpha_\ell, g_\ell\}_{\ell\in\mathcal{S}}} \quad \sum_{k=1}^{K}\sum_{t=0}^{T-1} f(\mathbf{p}^k, \mathbf{q}(t)) \tag{18a}$$

$$\text{s.t.} \quad \text{Power Flow Model (1)} \tag{18b}$$

$$\mathbf{q}(t+1) = \mathbf{q}(t) + \epsilon\left(\boldsymbol{\phi}(\mathbf{v}(t)) - \mathbf{q}(t)\right) \tag{18c}$$

$$\phi_i(\mathbf{v}) = \text{Proj}_{\mathcal{Q}_i}(-\nabla_{v_i} \sum_{\ell\in\mathcal{S}} g_\ell(\mathbf{v})), \forall i \in \mathcal{N} \tag{18d}$$

$$\{g_\ell\}_{\ell\in\mathcal{S}} \text{ are convex.} \tag{18e}$$

By parameterizing $\{g_\ell\}_{\ell\in\mathcal{S}}$ using ICNNs, problem (18) can be tractably solved using relevant learning algorithms.

V. Simulations

Here, we evaluate our approach on the reduced UCSD microgrid testbed [32] with different levels of communication. Though our theoretical analysis is based on the linearized power flow model, all experiments in this section are run using the nonlinear power flow simulator in Pandapower [33] to evaluate the algorithm performance.

A. UCSD Microgrid Testbed and the Dataset

The network model of the reduced UCSD microgrid testbed is shown in Fig. 4, showing the locations of the load and PV generators. This model consists of a total of 49 buses (including a substation bus), with 13 of them equipped with PV generators participating in voltage regulation. These are located at buses $\mathcal{C} = \{14, 15, 17, 19, 20, 27, 29, 30, 32, 34, 38, 39, 41\}$ and its nominal voltage magnitude is 12.47 kV. We provide in Table II (in Appendix) the network's equivalent resistances and reactances. We obtain the load and generation profiles of the UCSD microgrid by aggregating and scaling the real-gathered load and PV generation data at the UCSD campus [34] in Feb 2020. We normalize the aggregated building load profiles, and then obtain the active load profiles for each bus by scaling the normalized load profiles so that the demand peak across the network is about 1.8 times of the nominal demand (42

[1]We add the projection operator in (18d) to comply with the operational constraints in practical implementation, which is not considered in the theoretical analysis.

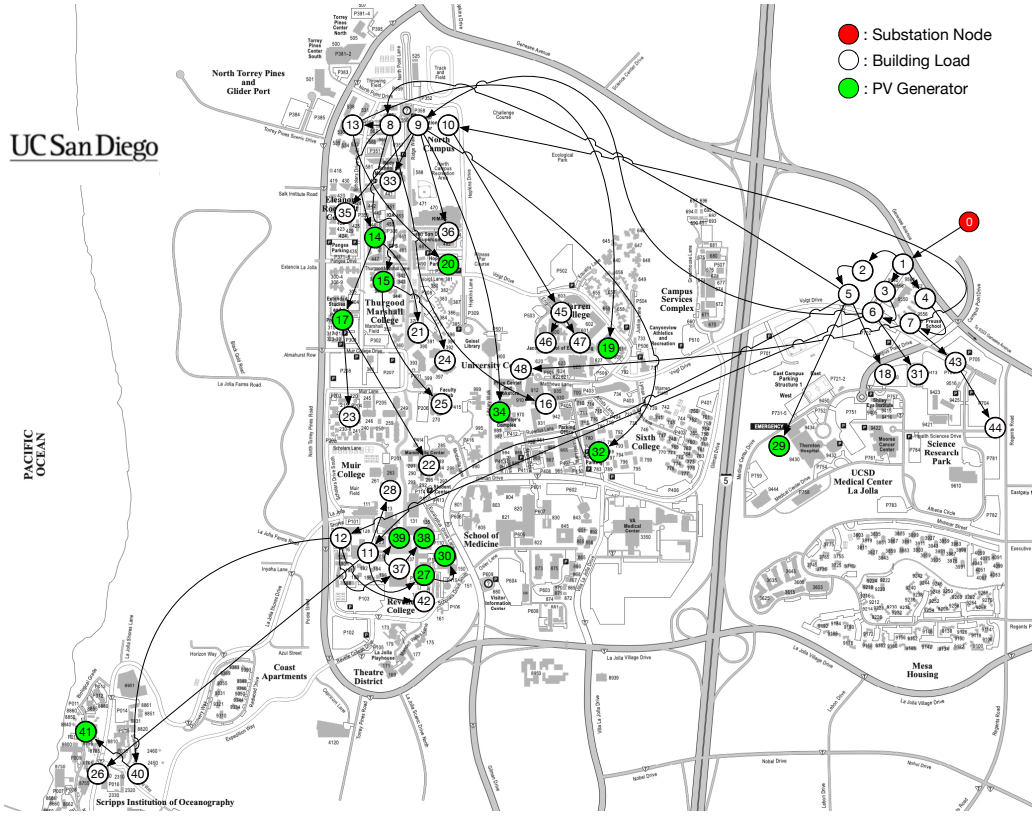

Fig. 4. Reduced-order model of the UCSD microgrid testbed with 13 PV generators equipped with voltage controllers located at nodes $\mathcal{C} = \{14, 15, 17, 19, 20, 27, 29, 30, 32, 34, 38, 39, 41\}$.

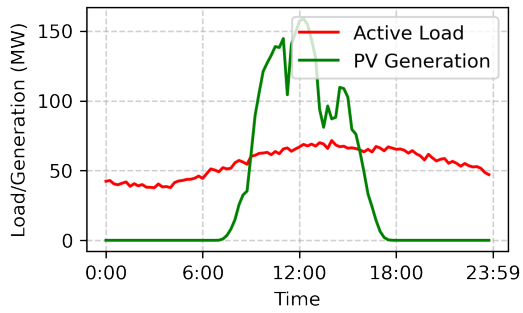

Fig. 5. The load and generation curves across the UCSD microgrid on February 2, 2020 (Sunday).

MW [32]). We synthesize the reactive load profiles according to the active load profiles and the power factors of the UCSD microgrid. Similarly, we obtain the active generation profiles for each PV generator by scaling the aggregated PV generation data to induce significant voltage deviations in high voltage scenarios ($> 5\%$). Fig. 5 illustrates an instance of the obtained load and generation curves across the network for one day (February 2, 2020). Each day consists of 96 data points, i.e., the data sampling period is 15 minutes. For training purpose, we generate three times more data for each day by adding 10% random noise to the 96 load and generation data points.

B. Controller and Training Setups

The controller setups with different communication levels are presented as follows:

- Controllers with No Communication: There is no communication, see Fig. 2(d). The communication network is partitioned into $S = 13$ communication subgraphs, with each controller only receives its local information. Each $\{g_\ell\}_{\ell\in\{1,..,13\}}$ is parameterized by an ICNN with two hidden layers, and each has 64 hidden units;
- Controllers with Distributed Communications: We consider two cases. For Case 1, each PV generator has a relatively small communication radius. The distributed communication network is shown in Fig. 6(a). The communication network is partitioned into $S = 5$ connected subgraphs, represented as $\mathcal{G}_1 = \{14, 15, 17, 20\}$, $\mathcal{G}_2 = \{19, 32, 34\}$, $\mathcal{G}_3 = \{27, 30, 38, 39\}$, $\mathcal{G}_4 = \{29\}$, and $\mathcal{G}_5 = \{41\}$. For Case 2, each PV generator has relatively larger communication radius, and the communication network is shown in Fig. 6(b). The communication network is partitioned into $S = 2$ connected subgraphs, represented as $\mathcal{G}_1 = \{14, 15, 17, 19, 20, 27, 29, 30, 32, 34, 38, 39\}$, $\mathcal{G}_2 = \{27, 30, 38, 39, 41\}$. Each $\{g_\ell\}_{\ell\in\{1,..,5\}}$ in the first cases and each $\{g_\ell\}_{\ell\in\{1,2\}}$ are all parameterized as an ICNN with two hidden layers, and each has 64 hidden units;
- Controllers with Full Communications: The communication network is all-to-all connected, see Fig. 2(a). The communication network is partitioned into $S = 1$ all-to-all connected subgraph, which contains all the 13 controlled buses. The only g_1 is parameterized using an ICNN with two hidden layers, and each has 64 hidden units.

For brevity, we use `Ctrl-NC`, `Ctrl-DC-1`, `Ctrl-DC-2`, and `Ctrl-FC` to represent the controllers under no com-

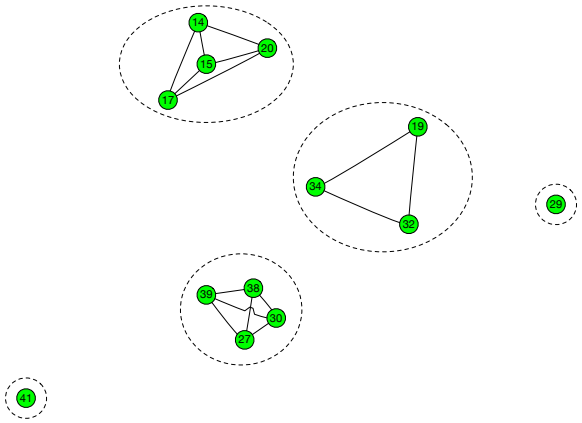

(a) Distributed communication network - Case 1

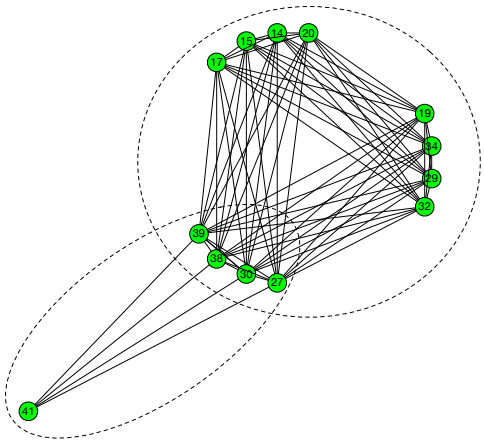

(b) Distributed communication network - Case 2

Fig. 6. Two different distributed Communication networks (we have slightly modified the relative physical location between buses to make the connectivity clearer). For Case 1/Case 2, the networks can be divided into five/two subgraphs (circled by dashed lines) which all have all-to-all communication.

munication, distributed communication - case 1, distributed communication - case 2, and full communication scenarios. We note that the overall communication level gradually increases for these four different communication scenarios, that is, `Ctrl-NC` < `Ctrl-DC-1` < `Ctrl-DC-2` < `Ctrl-FC`.

We use supervised learning to train the controllers parameterized by ICNNs. The goal is to make $\boldsymbol{\phi}$ approximate the OPF solutions at every step in (18). To achieve this, for each load and generation profile $\{\mathbf{p}^k, \mathbf{q}_{\mathcal{U}}^k\}_{k=1}^K$ in the dataset, we respectively compute the voltage magnitudes $\mathbf{v}_{\mathcal{C}}^k$ and the optimal reactive power setpoints $\mathbf{q}_{\mathcal{C}}^{\star,k}$ for the PV generators in $\mathcal{C}$ by solving the following OPF problem:

$$\begin{aligned} \min_{\mathbf{q}} \quad & f(\mathbf{p}^k, \mathbf{q}_{\mathcal{U}}^k, \mathbf{q}_{\mathcal{C}}) \\ \text{s.t.} \quad & \text{Power Flow Model (1)}, \mathbf{q} \in \mathcal{Q}. \end{aligned}$$

For the simulations here, we choose the cost function $f(\mathbf{p}, \mathbf{q}_{\mathcal{U}}, \mathbf{q})$ as:

$$100\|\mathbf{v}(\mathbf{p}, \mathbf{q}_{\mathcal{U}}, \mathbf{q}_{\mathcal{C}}) - \mathbf{1}\|^2 + \begin{bmatrix} \mathbf{q}_{\mathcal{U}}^\top & \mathbf{q}_{\mathcal{C}}^\top \end{bmatrix}^\top \mathbf{R} \begin{bmatrix} \mathbf{q}_{\mathcal{U}} \\ \mathbf{q}_{\mathcal{C}} \end{bmatrix},$$

where the first term is to penalize the voltage violations while the second term is to minimize the power losses induced by reactive power injections [4]. We refer to the first term as the *voltage deviation cost* and the second term *power loss cost*. We set the reactive power capability constraint $\mathcal{Q}$ to be $\{\mathbf{q}_{\mathcal{C}} : -\mathbf{q}_{\lim} \le \mathbf{q}_{\mathcal{C}} \le \mathbf{q}_{\lim}\}$, where $\mathbf{q}_{\lim} = [2,2,2,2,2,5,2,5,5,5,5,5,5]^\top$ (MVar).

By collecting the $\mathbf{v}_{\mathcal{C}}^k$ and $\mathbf{q}_{\mathcal{C}}^{\star,k}$ for all $k \in \{1,...,K\}$ into the labeled dataset, the supervised learning can be easily realized by solving $\min_{\boldsymbol{\phi}} \sum_{k=1}^K \|\mathbf{q}_{\mathcal{C}}^{\star,k} - \boldsymbol{\phi}(\mathbf{v}_{\mathcal{C}}^k)\|$ using relevant learning algorithms under different communication scenarios.

C. Simulation Results

We train the controllers using the load and generation data of the first 22 days in the dataset. To begin with, we analyze the trained controllers at buses 27 and 29 to gain an intuitive understanding of its behavior, as shown in Figure 7. The y-axis shows the outputs $\phi_{27}(\mathbf{v}_{\mathcal{C}}^k)$ and $\phi_{29}(\mathbf{v}_{\mathcal{C}}^k)$ under different communication scenarios for all $\{\mathbf{v}_{\mathcal{C}}^k\}_{k=1}^K$ in the labeled dataset as well as the OPF solutions. The OPF solutions, influenced by all buses across the network, demonstrates highly versatile behavior at a selected bus. This is called the *data inconsistency* phenomenon [12], as a fixed voltage magnitude at a single bus could have multiple different optimal control actions due to different status of other buses. Consequently, the `Ctrl-FC`, with global observation, closely aligns with the OPF solutions, while the `Ctrl-NC`, relying solely on local information, captures only the general trend. While for the `Ctrl-DC-1` and `Ctrl-DC-2`, with partial communication, achieve prediction accuracy between `Ctrl-FC` and `Ctrl-NC`. We also note that `Ctrl-DC-2` predicts better than `Ctrl-DC-1` as the former has a higher communication level compared to the latter. This also validates our statement in Remark III.4 that the control action for each bus is forced to be monotonically decreasing w.r.t. local voltage measurement for the `Ctrl-NC` to ensure closed-loop stability, and the inclusion of communication can break it to certain level to make the control action more flexible and accurate.

Next, we test the trained controllers in the UCSD microgrid using the load and generation data on February 29, 2020 (unseen during training) with 10% random noise. Specifically, we consider $T = 30$, i.e., for each data point, the reactive power iterations (2) run for 30 times, and the stepsize ϵ in controller (2) is selected to be 0.1. To show the effectiveness of the proposed framework, we compare in Fig. 8 the voltage trajectories for selected buses under the `Ctrl-DC-1` as well as `No Ctrl` and `OPF`, which represent the no control case and OPF case, respectively. It can be observed that compared to the `No Ctrl` case, the voltage deviations under `Ctrl-DC-1` are effectively mitigated, especially for low-voltage scenarios. To quantitatively compare the control performance under different communication scenarios, we provide the daily accumulated cost for different controllers in Table I. Since all controllers are trained using OPF solutions through supervised learning, they all achieve significant improvement compared to the `No Ctrl` case. Notably, as communication level increases, the overall performance steadily improves, and the behavior of the controller gradually become closer to the `OPF` solutions, in the sense that it tends to slightly increase the power loss cost for more significant reduction of voltage deviation cost.

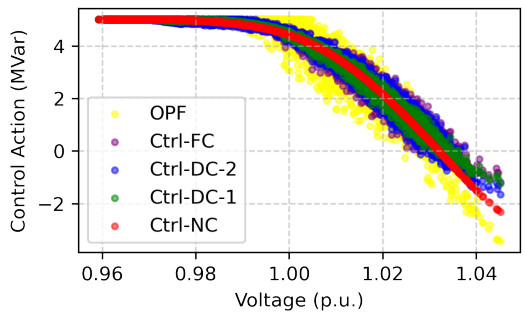

(a) Control actions at PV generator 27

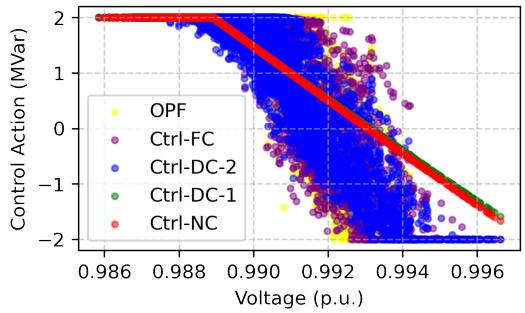

(b) Control actions at PV generator 29

Fig. 7. Control actions of the trained controllers at (a) bus 27 and (b) bus 29 under controllers with different communication scenarios.

TABLE I
ACCUMULATED COST ALONG THE DAY ON UCSD MICROGRID FOR CONTROLLERS UNDER DIFFERENT COMMUNICATION SCENARIOS.

Controller	Cost-Volt	Cost-Loss	Total Cost	Improvement
`No Ctrl`	2.0614	0.3143	2.3757	-
`Ctrl-NC`	0.6148	0.1571	0.7719	67.5%
`Ctrl-DC-1`	0.6001	0.1574	0.7575	68.1%
`Ctrl-DC-2`	0.5588	0.1623	0.7211	69.6%
`Ctrl-FC`	0.5334	0.1653	0.6987	70.6%
`OPF`	0.1883	0.2673	0.4556	80.8%

D. Discussion

The simulation results above illustrate the effectiveness of the proposed framework, and indicate that stronger communication capability helps enhance the performance of the designed voltage controllers in the DG. Particularly, we have the following interpretations and remarks:

- It can be observed that the `Ctrl-FC` still has a relatively large optimality gap compared to the `OPF` case. The reason is two-fold. First, even with full communication, the controllers still lack the information from the uncontrolled buses, while for the `OPF` case, the global information across the network is utilized. Second, the monotonicity requirement can introduce certain conservativeness when fitting to the OPF solutions. We note that there is a trade-off between theoretical guarantees (closed-loop stability) and the optimality of the controllers, as monotonicity is only a sufficient condition but not necessary for ensuring stability.
- In the simulations above, we do not explicitly highlight the closed-loop stability guarantees of the proposed framework. We note that this has been showcased in our prior works [9], [12] that without monotonicity constraints on the controllers, the learned controller may easily lead to instability issues for the closed-loop system, especially when the voltage magnitudes are significantly higher or lower than the nominal value.

VI. Conclusions and Future Work

We have presented a unified framework that allows us to design provably stable voltage controllers in distribution grids endowed with arbitrary communication infrastructures. The key enabler behind the proposed framework is that all local-acting controllers need to collectively satisfy a network-wide monotonicity condition, which ensures the closed-loop system is asymptotically stable. We have provided a design procedure that guarantees the derived local-acting controllers satisfy the network-wide monotonicity/stability condition under an arbitrary communication infrastructure and employed supervised learning to find the optimal ones. Simulation results with real-world data from the UCSD microgrid validate the effectiveness of the framework and reveal the role of communication in improving the control performance. Future work will include the theoretical characterization of the relationship between the connectivity of communication networks and control performance, which, from the experimental perspective, is that stronger connectivity implies better control performance. Other extensions include expanding the proposed framework to the case where active power is also controllable, adding safety limits of the voltage magnitudes during transient, and characterizing the region of attraction when taking into account the nonlinear power flow model.

References

[1] P. Srivastava, R. Haider, V. J. Nair, V. Venkataramanan, A. M. Annaswamy, and A. K. Srivastava, "Voltage regulation in distribution grids: A survey," *Annual Reviews in Control*, vol. 55, pp. 165–181, 2023.

[2] N. Li, G. Qu, and M. Dahleh, "Real-time decentralized voltage control in distribution networks," in *Allerton Conf. on Communications, Control and Computing*, (Monticello, IL, USA), pp. 582–588, Oct. 2014.

[3] H. Zhu and H. J. Liu, "Fast local voltage control under limited reactive power: Optimality and stability analysis," *IEEE Transactions on Power Systems*, vol. 31, no. 5, pp. 3794–3803, 2015.

[4] G. Cavraro and R. Carli, "Local and distributed voltage control algorithms in distribution networks," *IEEE Transactions on Power Systems*, vol. 33, no. 2, pp. 1420–1430, 2017.

[5] X. Zhou, M. Farivar, Z. Liu, L. Chen, and S. H. Low, "Reverse and forward engineering of local voltage control in distribution networks," *IEEE Transactions on Automatic Control*, vol. 66, no. 3, pp. 1116–1128, 2021.

[6] "IEEE standard for interconnection and interoperability of distributed energy resources with associated electric power systems interfaces," *IEEE Std 1547-2018 (Revision of IEEE Std 1547-2003)*, pp. 1–138, 2018.

[7] Y. Shi, G. Qu, S. H. Low, A. Anandkumar, and A. Wierman, "Stability constrained reinforcement learning for real-time voltage control," in *American Control Conference*, (Atlanta, GA), pp. 2715–2721, June 2022.

[8] W. Cui, J. Li, and B. Zhang, "Decentralized safe reinforcement learning for inverter-based voltage control," *Electric Power Systems Research*, vol. 211, p. 108609, 2022.

[9] J. Feng, Y. Shi, G. Qu, S. H. Low, A. Anandkumar, and A. Wierman, "Stability constrained reinforcement learning for decentralized real-time voltage control," *IEEE Transactions on Control of Network Systems*, vol. 11, no. 3, pp. 1370–1381, 2024.

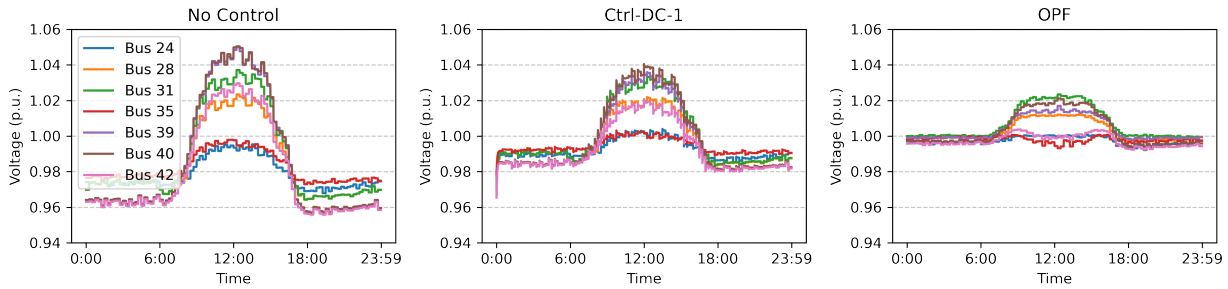

Fig. 8. Voltage trajectories for selected buses (buses 24, 28, 31, 35, 39, 40, 42) under the `No Ctrl`, `Ctrl-DC-1`, as well as `OPF` using the load and generation data on February 29, 2020 with random noise.

[10] J. Feng, W. Cui, J. Cortés, and Y. Shi, "Bridging transient and steady-state performance in voltage control: A reinforcement learning approach with safe gradient flow," *IEEE Control Systems Letters*, vol. 7, pp. 2845–2850, 2023.

[11] G. Cavraro, Z. Yuan, M. K. Singh, and J. Cortés, "Learning local Volt/Var controllers towards efficient network operation with stability guarantees," in *IEEE Conf. on Decision and Control*, (Cancun, Mexico), pp. 5056–5061, Dec. 2022.

[12] Z. Yuan, G. Cavraro, M. K. Singh, and J. Cortés, "Learning provably stable local Volt/Var controllers for efficient network operation," *IEEE Transactions on Power Systems*, vol. 39, no. 1, pp. 2066–2079, 2024.

[13] Z. Yuan, G. Cavraro, and J. Cortés, "Constraints on OPF surrogates for learning stable local Volt/Var controllers," *IEEE Control Systems Letters*, vol. 7, pp. 2533–2538, 2023.

[14] Z. Yuan, G. Cavraro, A. Zamzam, and J. Cortés, "Unsupervised learning for equitable DER control," *Electric Power Systems Research*, vol. 234, p. 110634, 2024.

[15] Q. Peng and S. H. Low, "Distributed optimal power flow algorithm for radial networks, I: Balanced single phase case," *IEEE Transactions on Smart Grid*, vol. 9, no. 1, pp. 111–121, 2016.

[16] S. Bolognani and S. Zampieri, "A distributed control strategy for reactive power compensation in smart microgrids," *IEEE Transactions on Automatic Control*, vol. 58, no. 11, pp. 2818–2833, 2013.

[17] B. Zhang, A. Y. S. Lam, A. D. Domínguez-García, and D. Tse, "An optimal and distributed method for voltage regulation in power distribution systems," *IEEE Transactions on Power Systems*, vol. 30, no. 4, pp. 1714–1726, 2014.

[18] S. Bolognani, R. Carli, G. Cavraro, and S. Zampieri, "Distributed reactive power feedback control for voltage regulation and loss minimization," *IEEE Transactions on Automatic Control*, vol. 60, no. 4, pp. 966–981, 2015.

[19] E. Dall'Anese and A. Simonetto, "Optimal power flow pursuit," *IEEE Transactions on Smart Grid*, vol. 9, no. 2, pp. 942–952, 2018.

[20] G. Qu and N. Li, "Optimal distributed feedback voltage control under limited reactive power," *IEEE Transactions on Power Systems*, vol. 35, no. 1, pp. 315–331, 2020.

[21] S. Gupta, A. Mehrizi-Sani, S. Chatzivasileiadis, and V. Kekatos, "Deep learning for scalable optimal design of incremental volt/var control rules," *IEEE Control Systems Letters*, vol. 7, pp. 2475–1456, 2023.

[22] I. Murzakhanov, S. Gupta, S. Chatzivasileiadis, and V. Kekatos, "Optimal design of Volt/VAR control rules for inverter-interfaced distributed energy resources," *IEEE Transactions on Smart Grid*, vol. 15, no. 1, pp. 312–323, 2024.

[23] A. Colot, E. Perotti, M. Glavic, and E. Dall'Anese, "Incremental Volt/Var control for distribution networks via chance-constrained optimization," *arXiv preprint arXiv:2405.02511*, 2024.

[24] M. E. Baran and F. F. Wu, "Optimal capacitor placement on radial distribution systems," *IEEE Transactions on Power Delivery*, vol. 4, no. 1, pp. 725–734, 1989.

[25] D. Deka, V. Kekatos, and G. Cavraro, "Learning distribution grid topologies: A tutorial," *IEEE Transactions on Smart Grid*, vol. 15, no. 1, pp. 999 – 1013, 2024.

[26] K. C. Border, *Fixed Point Theorems with Applications to Economics and Game Theory*. Cambridge, UK: Cambridge University Press, 1985.

[27] Z. Yuan, C. Zhao, and J. Cortés, "Reinforcement learning for distributed transient frequency control with stability and safety guarantees," *Systems & Control Letters*, vol. 185, p. 105753, 2024.

[28] K. Turitsyn, P. Sulc, S. Backhaus, and M. Chertkov, "Options for control of reactive power by distributed photovoltaic generators," *Proceedings of the IEEE*, vol. 99, no. 6, pp. 1063–1073, 2011.

[29] R. A. Horn and C. R. Johnson, *Matrix Analysis*. New York, USA: Cambridge University Press, 2012.

[30] W. Cui, Y. Jiang, B. Zhang, and Y. Shi, "Structured neural-PI control with end-to-end stability and output tracking guarantees," in *Conference on Neural Information Processing Systems*, (New Orleans, LA, USA), Dec. 2023.

[31] B. Amos, L. Xu, and J. Z. Kolter, "Input convex neural networks," in *International Conference on Machine Learning*, (Sydney Australia), pp. 146–155, Aug. 2017.

[32] B. Washom, J. Dilliot, D. Weil, J. Kleissl, N. Balac, W. Torre, and C. Richter, "Ivory tower of power: Microgrid implementation at the University of California, San Diego," *IEEE Power and Energy Magazine*, vol. 11, no. 4, pp. 28–32, 2013.

[33] L. Thurner, A. Scheidler, F. Schafer, J. H. Menke, J. Dollichon, F. Meier, S. Meinecke, and M. Braun, "Pandapower - An open source python tool for convenient modeling, analysis and optimization of electric power systems," *IEEE Transactions on Power Systems*, vol. 33, no. 6, pp. 6510–6521, 2018.

[34] S. Silwal, C. Mullican, Y.-A. Chen, A. Ghosh, J. Dilliott, and J. Kleissl, "Open-source multi-year power generation, consumption, and storage data in a microgrid," *Journal of Renewable and Sustainable Energy*, vol. 13, no. 2, p. 025301, 2021.

APPENDIX

TABLE II
UCSD MICROGRID LINE PARAMETERS.

From	To	$r_{mn}(\Omega)$	$x_{mn}(\Omega)$	From	To	$r_{mn}(\Omega)$	$x_{mn}(\Omega)$
0	1	0.0174	0.0002	15	25	0.7802	1.1703
1	2	0.0232	0.4855	11	26	0.2722	0.3906
1	3	0.0238	0.4894	11	27	0.4659	0.6989
1	4	0.0232	0.4778	11	28	0.4659	0.0002
2	5	0.0185	0.0278	5	29	0.1126	0.2166
3	6	0.0255	0.0382	27	30	0.3496	0.5244
4	7	0.0324	0.0486	6	31	0.5803	0.8704
5	8	0.5452	0.8178	9	32	0.2547	0.3820
6	9	0.4376	0.6563	9	33	0.5093	0.7640
7	10	0.4352	0.6529	9	34	0.3478	0.5218
5	11	0.9417	1.4125	9	35	0.2722	0.3906
6	12	0.9000	1.3500	9	36	0.2722	0.0002
8	13	0.9000	0.0005	12	37	0.0324	0.0486
8	14	0.5961	0.8942	37	38	0.7802	1.1703
8	15	0.6338	0.9506	37	39	0.3700	0.3717
8	16	0.1922	0.2882	12	40	0.1105	0.1658
14	17	0.2275	0.3412	40	41	0.1109	0.2132
5	18	0.1160	0.2230	12	42	0.1922	0.2882
13	19	0.1268	0.1901	7	43	0.1175	0.1762
13	20	0.3478	0.5218	43	44	0.0191	0.0286
14	21	0.0174	0.0260	10	45	0.4457	0.6685
17	22	0.1256	0.1884	45	46	0.0868	0.1302
17	23	0.0174	0.0260	45	47	0.1105	0.1658
15	24	0.3531	0.5296	7	48	0.0301	0.0451